Pure Appl. Geophys. 173 (2016), 1115–1124

DOI 10.1007/s00024-015-1160-4

Pure and Applied Geophysics

Potential Misidentification of Love-Wave Phase Velocity Based on Three-Component Ambient Seismic Noise

Zongbo Xu,[1] Jianghai Xia,[1,2] Yinhe Luo,[2] Feng Cheng,[1] and Yudi Pan[1]

Abstract—People have calculated Rayleigh-wave phase velocities from vertical component of ambient seismic noise for several years. Recently, researchers started to extract Love waves from transverse component recordings of ambient noise, where "transverse" is defined as the direction perpendicular to a great-circle path or a line in small scale through observation sensors. Most researches assumed Rayleigh waves could be negligible, but Rayleigh waves can exist in the transverse component when Rayleigh waves propagate in other directions besides radial direction. In study of data acquired in western Junggar Basin near Karamay city, China, after processing the transverse component recordings of ambient noise, we obtain two energy trends, which are distinguished with Rayleigh-wave and Love-wave phase velocities, in the frequency–velocity domain using multichannel analysis of surface waves (MASW). Rayleigh waves could be also extracted from the transverse component data. Because Rayleigh-wave and Love-wave phase velocities are close in high frequencies (>0.1 Hz), two kinds of surface waves might be merged in the frequency–velocity domain. Rayleigh-wave phase velocities may be misidentified as Love-wave phase velocities. To get accurate surface-wave phase velocities from the transverse component data using seismic interferometry in investigating the shallow geology, our results suggest using MASW to calculate real Love-wave phase velocities.

Key words: Surface-wave phase velocity, seismic interferometry, multichannel analysis of surface waves.

1. Introduction

Ambient seismic noise contains surface waves (Shapiro and Campillo 2004) and body waves (e.g., Roux *et al.* 2005; Wang *et al.* 2014a). It is more convenient to extract surface waves from ambient noise, however, because surface waves possess higher energy than body waves. Nowadays, ambient noise is widely used to extract surface waves in research (Shapiro *et al.* 2005) and engineering (Park *et al.* 2007; Lin *et al.* 2013). Rayleigh waves could be extracted in two main methods: spatial autocorrelation method (SPAC) and seismic interferometry. The common features of the two methods have been studied (Prieto *et al.* 2009; Tsai and Moschetti 2010).

SPAC method was firstly proposed by Aki (1957) with sensors arrayed in a circle. Sensor-array was simplified into line (Chávez-García *et al.* 2006; Margaryan *et al.* 2009) and even only two sensors (Morikawa *et al.* 2004; Chávez-García *et al.* 2005). It has been demonstrated that reliable Rayleigh-wave phase velocities would be calculated with two sensors using SPAC method (Boschi *et al.* 2013).

Seismic interferometry, including cross-correlation and cross-coherence, has been used to generate empirical Green's functions from ambient seismic noise (Weaver and Lobkis 2001; Campillo and Paul 2003). Rayleigh-wave group velocities and phase velocities can be calculated through the empirical Green's function between two sensors (Shapiro *et al.* 2005; Yao *et al.* 2006). Xu *et al.* (2013) used multichannel analysis of surface waves (MASW) (e.g., Song *et al.* 1989; Xia 2014) in imaging surface waves by processing the empirical Green's functions while investigated the near surface.

Love waves could also be extracted from three-component data or transverse component data using seismic interferometry (Nakata *et al.* 2011; Behm and Snieder 2013). While analyzing the transverse component of empirical Green's functions, people used to

[1] Subsurface Imaging and Sensing Laboratory, Institute of Geophysics and Geomatics, The China University of Geosciences, 388 Rumo Rd., Wuhan, Hubei 430074, China. E-mail: jianghai_xia@yahoo.com; jxia@cug.edu.cn

[2] Hubei Subsurface Multi-scale Imaging Key Laboratory, Institute of Geophysics and Geomatics, The China University of Geosciences, 388 Rumo Rd., Wuhan, Hubei 430074, China.

focus on Love waves and neglect Rayleigh waves. In real ambient noise, however, there are not only Love waves but also Rayleigh waves propagating in horizontal directions (Aki 1957). Noise sources were assumed distributed randomly (Arai and Tokimatsu 2004). Because some noise sources are distributed away from the radial direction, the horizontal components of Rayleigh waves which are stimulated by the noise sources could be decomposed to the transverse component. As a result, we could observe both Love waves and Rayleigh waves in the transverse direction (Okada 2003). Through analyzing the transverse component of empirical Green's functions, both Rayleigh waves and Love waves would be distinguished in the frequency–velocity (*f-v*) domain.

In this study, we process broadband three-component ambient noise acquired in Xinjiang Province, China, using SPAC and seismic interferometry. Rayleigh-wave phase velocities are calculated through the two methods. We then focus on analyzing transverse component of empirical Green's functions in theory and practice. The transverse component of empirical Green's functions is analyzed in the *f-v* domain using the MASW method. Both Rayleigh waves and Love waves are found in the *f-v* domain as theory indicates. At last, we discuss influence of Rayleigh waves existing in the transverse component data.

2. Data Acquisition

Ambient seismic noise data were recorded in western Junggar Basin near Karamay city, China, in this study for reconnaissance of mineral resources and delineating deep-seated structures (Liu *et al.* 2014; He *et al.* 2015). The study site (Fig. 1) includes deserts, a river, roads, and Karamay city. Deserts are the main observation site, where there are few human activities. A river and several roads cross the survey line, which is plotted with red triangles (Fig. 1). Although ambient noises may be due to the flowing river and moving cars on the roads, the main noise source is from the city where people's activities and traffic noise are strong enough to produce seismic noise in 1–5 Hz (Wang *et al.* 2014b).

Karamay downtown is located 5 km away from the east end of the survey line. The survey line is 70 km long and about 76° from the north to the east (NE). The entire survey line was covered by 35 broadband three-component seismometers (120 s to 50 Hz) with a 1 km interval in three rounds. The 71 observation points in total were named W00, W01 to W70 (red triangles in Fig. 1). Each round was overlapped with a distance about 17 km and lasted around 16 days. Seismometers recorded ambient seismic noise in vertical, north and east directions at a 100 Hz sampling rate.

3. Calculating Rayleigh-Wave Phase Velocities

Vertical component of ambient noise is dominated by Rayleigh-wave energy. Rayleigh-wave phase velocities have always been calculated by processing the vertical component data (Aki 1957; Lin *et al.* 2008). We process the vertical component data by referring to the procedures proposed by Bensen *et al.* (2007) in three steps: data preparation, cross-coherence, and phase velocity measurement.

3.1. Data Preparation

Means and trends of raw data are removed in data preparation. To remove waves outside the target frequency band (0.5–5 Hz), band-pass filter between 0.1 and 15 Hz is applied to the data. Then the data are cut into same window-length (1 h) sections. Large events (such as earthquakes) are removed using temporal normalization with an iterative water-level normalization algorithm discussed by Bensen *et al.* (2007). We set three times of standard deviation as the water-level, and down-weight amplitude above it iteratively until the entire waveform is below the water-level. Using this method, the amplitude could be fully preserved if there are no big earthquakes in raw data (Fig. 2). Even if earthquakes are obvious in raw data (Fig. 3a) and after band-pass filtering (Fig. 3b), they will disappear through the temporal normalization (Fig. 3c, d).

3.2. Cross-Coherence

Cross-coherence is calculated between two sensors (for example, *A* and *B*). We calculate the spectral

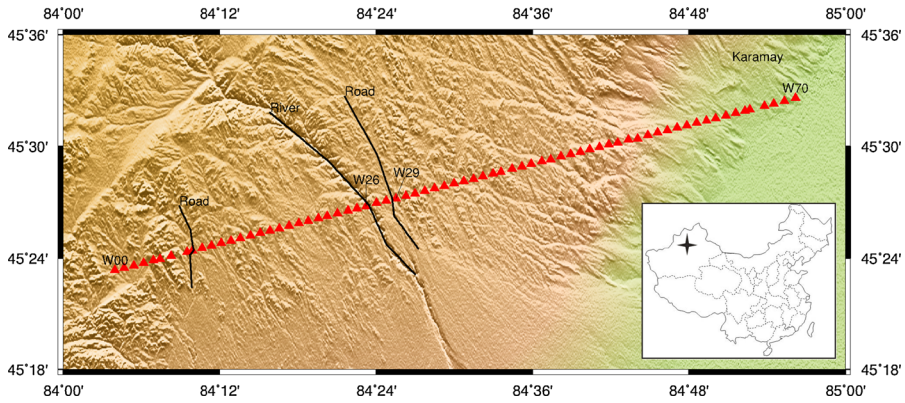

Figure 1
A site map of the study field. Each *red triangle* represents an observation point. A river and roads are pointed out with *black line*. The insects show the geographical location of the study site in China with the *black star*

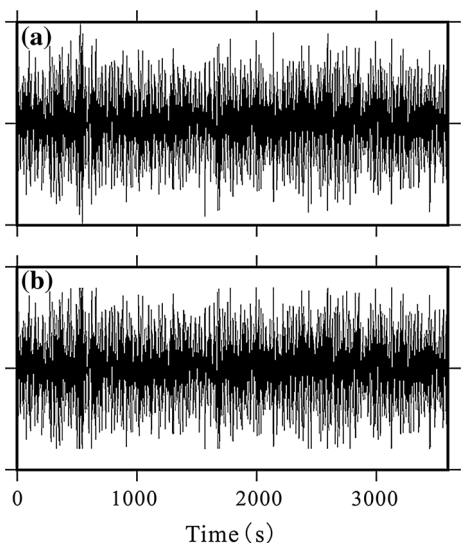

Figure 2
Data before and after temporal normalization. **a** After a mean and a trend are removed from raw data, the data are band-pass filtered between 0.1 and 15 Hz. **b** The data in **a** are temporal normalized

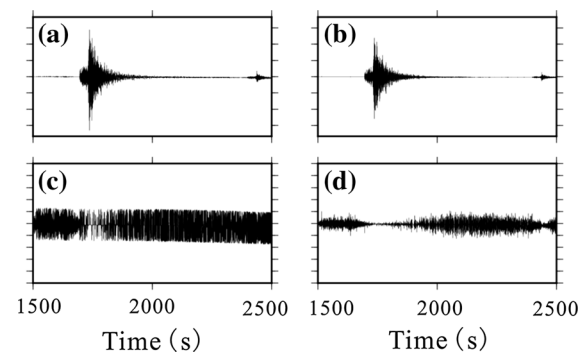

Figure 3
The record containing earthquakes before and after temporal normalization. **a** The record is processed as Fig. 2a. **b** The data in **a** are band-pass filtered between 0.5 and 5 Hz. The signal of earthquakes still remains in the band. **c** The data in **a** are temporal normalized. The signal of earthquakes disappears. **d** The data in **c** are band-pass filtered between 0.5 and 5 Hz. The earthquakes are still invisible. So the signal of earthquake is removed fully

cross-coherence $H_{AB,i}$ of ith time-window section with following equation:

$$H_{AB,i} = \frac{u_{A,i}u^*_{B,i}}{|u_{A,i}||u_{B,i}|} \quad (1)$$

where $u_{A,i}$ is spectrum of sensor A's ith time-window record and asterisk denotes a complex conjugate. Here we adopt cross-coherence instead of cross-correlation, because cross-coherence possesses better ability to reduce the influence of random noise (NAKATA *et al.* 2011). Equation 1 indicates that cross-coherence could be recognized as pre-whitening plus cross-correlation in the frequency domain (PRIETO *et al.* 2009). The cross-coherences $H_{AB,i}$ are stacked to obtain final results H_{AB} with following equation:

$$H_{AB} = \sum_{i}^{N} H_{AB,i} \quad (2)$$

where N is the total number of time-window sections.

3.3. Phase Velocity Measurement

Phase velocity could be calculated from the final result H_{AB} in the frequency domain and the time

domain. In the frequency domain, the real part of averaged cross-coherence is SPAC coefficient $\overline{\rho}(\omega, r)$ (Fig. 4a) (Chávez-García *et al.* 2005; Ekström *et al.* 2009) and the SPAC coefficient is equal to $J_0\left(\frac{\omega r}{c(\omega)}\right)$ as following equation (Aki 1957; Okada 2003):

$$\overline{\rho}(\omega, r) = \text{Real}\left(\frac{1}{N} H_{AB}(\omega)\right) = J_0\left(\frac{\omega r}{c(\omega)}\right) \tag{3}$$

where J_0 is the Bessel function of the first kind, zero order, r is distance between two sensors (A and B), and $c(\omega)$ is phase velocity at frequency ω. Phase velocity could be calculated using the frequency of zero crossings (Ekström *et al.* 2009; Luo *et al.* 2012), crests and troughs (Aki 1957) in the SPAC coefficients with equation

$$c(\omega_n) = \frac{\omega_n r}{z_n} \tag{4}$$

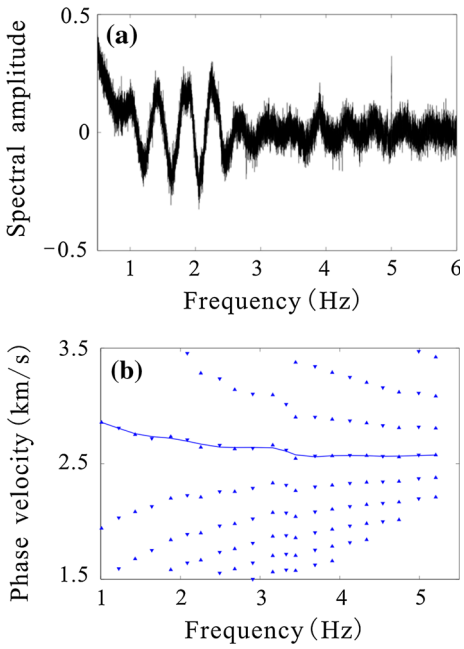

Figure 4
Calculating Rayleigh-wave phase velocities through SPAC method. **a** The real part of averaged spectral cross-coherence between W37 and W43. **b** *Triangles* represent calculated results of Eq. 5. *Upward triangles* represent crests in **a**, and *downward triangles* represent troughs in **a**. According to the range of Rayleigh-wave phase velocity (from 3 to 2.5 km/s, between 1 and 5 Hz in this area), *triangles near the blue line* are appropriate and selected as Rayleigh-wave phase velocities. The *blue line* represents the smooth results of the selected phase velocities

where ω_n denotes the frequency of the nth observed zero crossing, crest or trough and z_n denotes the nth observed zero crossing, crest or trough of J_0. In practice, because random noise in spectrum could cause missed or extra zero crossings, crests or troughs, a set of estimated $c_m(\omega_n)$ based on Eq. 4 are calculated

$$c_m(\omega_n) = \frac{\omega_n r}{z_{n+2m}} \tag{5}$$

where m equals 0, ± 1, ± 2,…, indicating the number of the missed or extra ones (Ekström *et al.* 2009).

We choose crests and troughs instead of zero crossings to calculate phase velocity, because crests and troughs could be detected from random noise with their high amplitude. Using Eq. 5, a set of phase velocities could be calculated (Fig. 4b). Because Rayleigh waves dominate in the vertical component data, the calculated phase velocities are mainly due to Rayleigh waves. We identify fundamental mode Rayleigh-wave phase velocities (triangles near the blue line in Fig. 4b) within a reasonable range (from 3 to 2.5 km/s, from 1 to 5 Hz in this area).

Stacked cross-coherence $H_{AB}(t)$ in the time domain could be used to generate empirical Green's function $G_{AB}(t)$ (Snieder 2004; Lin *et al.* 2008) with

$$G_{AB}(t) = -\frac{\mathrm{d}H_{AB}(t)}{\mathrm{d}t} 0 \le t < \infty. \tag{6}$$

This step could also enhance signal at high frequencies (Sabra *et al.* 2005a, b).

Green's function between two sensors could be recognized as shooting at one sensor, recording at the other. The vertical component of empirical Green's functions between a certain and several other sensors could be formed as a common-shot gather (Fig. 5a), where surface waves can be observed clearly. The pseudo shot-gather is transformed into the f-v domain using high-resolution linear Radon transform (Luo *et al.* 2008). A continuous energy trend can be seen in the f-v domain (Fig. 5b), and phase velocities could be picked by following the energy peak.

It is well known that the imaginary part of spectral Green's function for Rayleigh waves has the shape of a Bessel function in a homogeneous medium (Tsai and Moschetti 2010; Boschi *et al.* 2013). So seismic interferometry and SPAC could generate similar

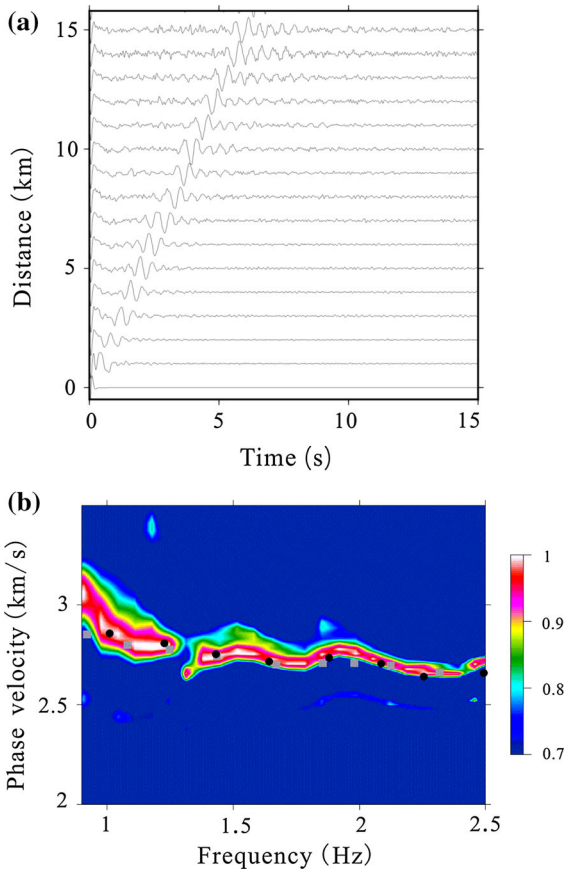

Figure 5
a The *vertical* component of empirical Green's functions (band-pass filtered between 0.5 and 5 Hz) between W30 and W30 to W45 are arrayed. **b** The pseudo shot-gather in **a** (where W30 is a virtual shooting point, W37 to W43 are receivers) is analyzed in the *f-v* domain. The energy trend is calculated using high-resolution linear Radon transform (Luo *et al.* 2008) and represents Rayleigh waves. *Black dots* represent results calculated through SPAC method and *gray squares* represent results calculated by Yao's method (Yao *et al.* 2006)

phase velocity in a homogeneous medium. Particularly, in this study, Rayleigh-wave phase velocities obtained through the two methods show good consistency (Fig. 5b).

The reliability of the obtained Rayleigh-wave phase velocities is further ensured by comparing the obtained and results of another method (Yao *et al.* 2006). The Rayleigh-wave phase velocities estimated using Yao's method also agree well with results of seismic interferometry and SPAC (Fig. 5b). It is obvious that we could obtain similar Rayleigh-wave phase velocities through these three different methods.

4. Calculating Love-Wave Phase Velocities

4.1. Theory

People usually extract Love waves from the transverse component that is perpendicular to the direction of a great-circle path or a line in small scale through observation sensors in ambient seismic noise (Lin *et al.* 2008; Nakata *et al.* 2011). The transverse component data contain Rayleigh waves and Love waves (Okada 2003). If the transverse component data of two sensors (for example, A and B) are processed with seismic interferometry, the equation of seismic interferometry in the frequency domain (here we use cross-correlation as example) is as followings:

$$\begin{aligned}&\sum_{i}^{N} u_{A,i}u_{B,i}^{*}\\&\quad=\sum_{i}^{N}\left[(u_{A,R,i}+u_{A,L,i})(u_{B,R,i}^{*}+u_{B,L,i}^{*})\right]\\&\quad=\sum_{i}^{N}(u_{A,R,i}u_{B,R,i}^{*}+u_{A,R,i}u_{B,L,i}^{*}\\&\qquad+u_{A,L,i}u_{B,R,i}^{*}+u_{A,L,i}u_{B,L,i}^{*})\end{aligned}\tag{7}$$

where $u_{A,R,i}$ and $u_{A,L,i}$ indicates the spectrum of Rayleigh waves and Love waves in the transverse record within sensor A's ith time-window section. Here we only deal with Rayleigh waves and Love waves included in the transverse component data and neglect other irregular or weak noise. Rayleigh waves and Love waves are assumed to be mutually uncorrelated (Okada 2003; Cho *et al.* 2006). So Eq. 7 can be further derived as

$$\begin{aligned}&\sum_{i}^{N}\left(u_{A,R,i}u_{B,R,i}^{*}+u_{A,R,i}u_{B,L,i}^{*}+u_{A,L,i}u_{B,R,i}^{*}+u_{A,L,i}u_{B,L,i}^{*}\right)\\&\approx\sum_{i}^{N}\left(u_{A,R,i}u_{B,R,i}^{*}+u_{A,L,i}u_{B,L,i}^{*}\right)\end{aligned}\tag{8}$$

Rayleigh waves and Love waves exist in the cross-correlation of the transverse component data (Eq. 8). The two kinds of waves also exist in cross-coherence, because whitened cross-correlation is equivalent to cross-coherence (Prieto *et al.* 2009);

it has been proven that there are the two kinds of waves in the real part of spectral cross-coherence for the transverse component (Aki 1957; Okada 2003; Cho *et al.* 2006). So the transverse component of empirical Green's function also includes the two kinds of waves.

4.2. Practice

To demonstrate this phenomenon, we analyze the transverse component of empirical Green's functions in the *f-v* domain and distinguish Rayleigh waves and Love waves.

The transverse component of ambient seismic noises is acquired through observation in transverse direction (Nakata *et al.* 2011) or recovering from north and east components (Lin *et al.* 2008; Behm and Snieder 2013). Here we rotate north and east components (N and E) into the transverse component (T) with following equation:

$$T = N\cos\theta - E\sin\theta \tag{9}$$

where θ represents the angle between direction of the survey line and east direction (Fig. 6).

By processing the transverse component data with the same procedures of seismic interferometry discussed in the previous sections, we could achieve empirical Green's functions. The empirical Green's functions are arrayed to form a pseudo shot-gather (Fig. 7a). The dispersion image in the *f-v* domain presents two dispersion energy trends. The two energy trends suggest two kinds of dispersive waves which possess different velocities at each frequency (Fig. 7b). The two kinds of surface waves will be demonstrated to be Rayleigh waves and Love waves with determined Rayleigh-wave and Love-wave phase velocities in the followings.

Rayleigh-wave phase velocities obtained using vertical component data through SPAC (black dots in Fig. 7b) are very close to the lower-velocity energy trend. It indicates that the lower-velocity energy trend represents Rayleigh waves. So the energy of Rayleigh waves exists in the transverse component of empirical Green's functions.

With the Rayleigh-wave phase velocities (Fig. 5b), we could obtain a multi-layer shear-wave velocity model (Xia *et al.* 1999) as the inversion

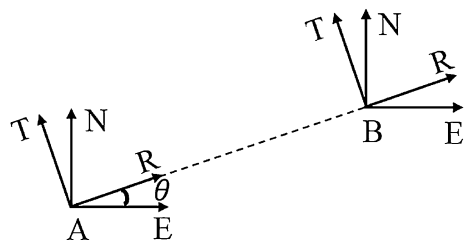

Figure 6
Illustration of how transverse (T) component is defined between two sensors (A and B)

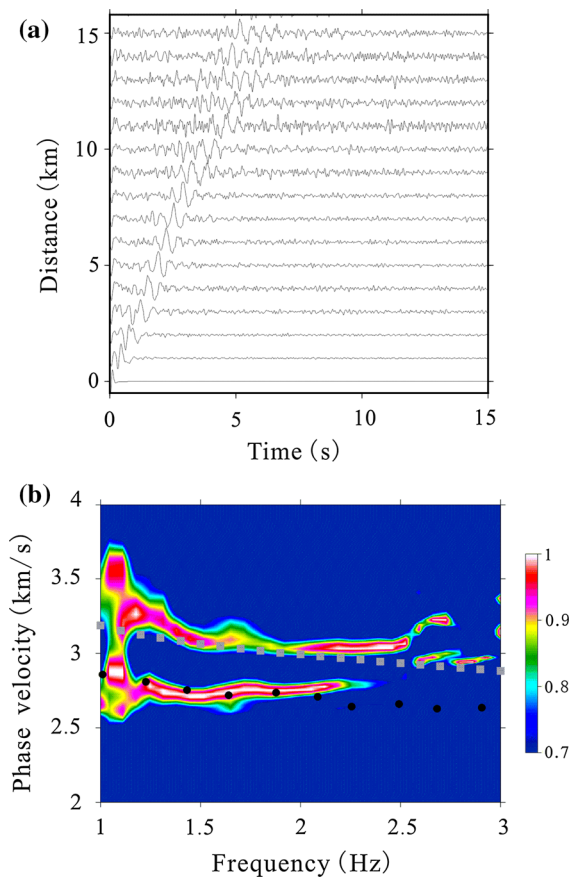

Figure 7
a The *transverse* component of empirical Green's functions (band-pass filtered between 0.5 and 5 Hz) between W33 and W33 to W48 are arrayed. **b** The pseudo shot-gather in **a** (where W33 is a virtual shooting point, W37 to W43 are receivers) is analyzed in the *f-v* domain using high-resolution linear Radon transform (Luo *et al.* 2008). *Black dots* represent the Rayleigh-wave phase velocities calculated in Fig. 4b; *gray squares* represent the forward calculated Love-wave phase velocities discussed in Sect. 4.2

result, then Love-wave phase velocities (gray squares in Fig. 7b) can be calculated through forward modeling (Schwab and Knopoff 1970). The forward calculated Love-wave phase velocities agree with velocity of the higher-velocity energy trend, indicating that the higher-velocity energy trend is due to Love waves.

As Fig. 7b shows, the two energy trends are close to each other. So these two trends would merge and probably be misidentified as one trend (the energy trend in Fig. 8) with methods (such as Yao *et al.*'s method 2006) that neglect Rayleigh waves exist. The misidentified energy trend would be the mixture of Love waves and Rayleigh waves, instead of true Love waves. As a result, slightly lower Love-wave phase velocities and an inversion result with lower shear-wave velocity would be obtained.

5. Discussion

5.1. Assessing Bias in Phase Velocities

There would be bias in measured surface-wave phase velocities from the real ones due to uneven ambient energy noise distribution (Yang and Ritzwoller 2008). The bias is found to be slight and below 5 % (Yao and van Der Hilst 2009). The bias could be smaller if more noise sources were within the Fresenel zone where plane waves propagate with an angle aside the direction of a survey line (the angle is from 0° to 28.9° and from 331.1° to 360° in a homogeneous media), because energy of noise sources in the Fresenel zone controls recovering empirical Green's function (Yao and van Der Hilst 2009). Besides noise sources distributed in the Fresenel zone, long time recording and 2D array could also reduce the bias in measured surface-wave phase velocities (Aki 1957; Yao and van Der Hilst 2009).

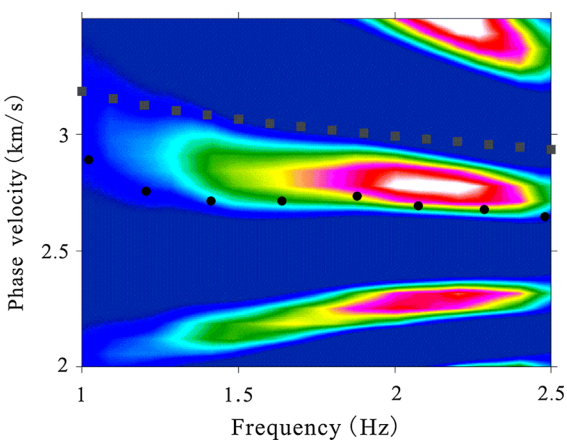

Figure 8
Love waves imaging using Yao's method (2006) with the empirical Green's function between W37 and W43. *Black dots* represent the Rayleigh-wave phase velocities calculated in Fig. 4b; *gray squares* represent the forward calculated Love-wave phase velocities discussed in Sect. 4.2

In our study site, the main noise source is found to be the Karamay city based on the results of beamforming analysis (Wang *et al.* 2014b). Because the city is distributed in the Fresenel zone of the survey line (Fig. 1), the obtained Rayleigh-wave and Love-wave phase velocities are reliable. Inverted multilayer shear-wave velocity models are also reliable due to the stability of inversion (Xia *et al.* 1999).

5.2. Calculating Real Love-Wave Phase Velocities

Methods that neglect Rayleigh waves exist would misidentify Love-wave phase velocities dealing with the transverse component of ambient seismic noise in this paper. Those methods are based on one empirical Green's function between two sensors. Waveforms of surface waves in the empirical Green's function are important for calculating phase velocity of the surface waves (Yao *et al.* 2006; Lin *et al.* 2008). Because the phase velocities of Rayleigh and Love waves are close at high frequencies (>0.1 Hz) and distance between two sensors in this paper is short (e.g., 6 km), arrival times of the two kinds of waves are very close. As a result, the waveforms of Love waves and Rayleigh waves would be merged (Fig. 9). There is only one peak of waveforms (red line in Fig. 9) in the transverse component near the peak of Rayleigh waves in the vertical component (black line in Fig. 9). So the waveforms in the transverse component must include the two kinds of waves. Information of Love waves may not be identified in the waveforms of single empirical Green's function so that true Love-wave phase velocities could hardly be calculated. Love-wave phase velocities, which are slightly lower than the real ones, could be obtained using those methods at high frequencies in this study.

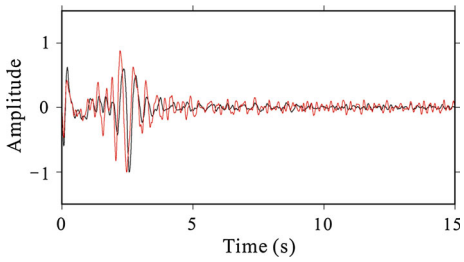

Figure 9
The *transverse* component (*red line*) of empirical Green's function extracted from the *transverse* component data and the *vertical* component (*black line*) of empirical Green's function extracted from the *vertical* component data between W37 and W43. Both are band-pass filtered between 0.5 and 5 Hz, and normalized

Those methods (Yao *et al.* 2006; Lin *et al.* 2008) based on one Green's function could only calculate fundamental Rayleigh-wave or Love-wave phase velocities, but MASW is based on several Green's functions. And MASW could image different surface waves, like fundamental and higher-mode surface waves, in the *f-v* domain simultaneously (Xia *et al.* 2003). So we adopt MASW to obtain Love-wave phase velocities in the frequency band (0.5–5 Hz). As a result, Rayleigh waves and Love waves could both be imaged (Fig. 7b). Love waves at high frequencies are important in investigating the shallow geology while the distance between sensors is limited to several hundred meters, even meters. MASW is suitable for calculating Love-wave phase velocities in investigating the near surface. MASW does require dense networks of sensors, and this requirement could be easily met in investigating the shallow geology.

It does not mean that true Love-wave phase velocity could not be calculated using those methods (Yao *et al.* 2006; Lin *et al.* 2008) in other situations. When ambient seismic noise in a low frequency band (e.g., 0.01–0.1 Hz) is researched and the distance between sensors is several hundred kilometers, the velocities of Rayleigh and Love waves are in large difference. In this situation, the arrival times and waveforms of the two kinds of waves could be distinctively separated from each other.

6. Conclusions

Rayleigh waves and Love waves both could be extracted from the transverse component data using seismic interferometry, because horizontal components of ambient seismic noise possess the two kinds of waves. We demonstrate it in both theory and practice.

Rayleigh waves and Love waves can be imaged in the *f-v* domain after processing the transverse component data in this paper. Rayleigh-wave and Love-wave phase velocities are so close at high frequencies that the energy of two waves could merge in the *f-v* domain. If we neglect Rayleigh waves, the merged energy trend may be misidentified as Love waves. Consequently, we would calculate Love-wave phase velocities which are slightly lower than the real ones in this study, which results in a multi-layer model with lower shear-wave velocities after inversion.

We recommend, in investigating the shallow geology, using MASW with the high-resolution linear Radon transform (Luo *et al.* 2008) to calculate real Love-wave phase velocities from the results of seismic interferometry.

Acknowledgments

We appreciate the Editor Arthur Snoke and three anonymous reviewers for their constructive and detailed comments and suggestions. This study is supported by the project "Deep Geological Investigation of the Karamay Back Mountain Area in Western Junggar, Xinjiang", China Geological Survey under Grant No. 1212011220245, the National Natural Science Foundation of China under Grant No. 41274142, and the Program of Introducing Talents of Discipline to Universities (Grant No. B14031). We also appreciate Shuttle Radar Topography Mission (SRTM) for providing digital elevation data and Chao Shen for providing software (SurfWave) in surface-wave imaging.

References

Aki, K. (1957), *Space and time spectra of stationary stochastic waves, with special reference to microtremors*, Bull. Earthq. Res. Inst. Tokyo University *35*, 415–456.

Arai, H., and Tokimatsu, K. (2004), *S-wave velocity profiling by inversion of microtremor H/V spectrum*, Bull. Seismol. Soc. Am. *94*(1), 53–63.

Behm, M., and Snieder, R. (2013), *Love waves from local traffic noise interferometry*, The Leading Edge *32*(6), 628–632.

Bensen, G.D., Ritzwoller, M.H., Barmin, M.P., Levshin, A.L., Lin F., Moschetti, M.P., and Yang, Y. (2007), *Processing seismic ambient noise data to obtain reliable broad-band surface wave dispersion measurements*, Geophys. J. Internat. *169*(3), 1239–1260.

Boschi, L., Weemstra, C., Verbeke, J., Ekström, G., Zunino, A., and Giardini, D. (2013), *On measuring surface wave phase velocity from station–station cross-correlation of ambient signal*, Geophys. J. Internat. *192*(1), 346–358.

Campillo, M., and Paul, A. (2003), *Long-range correlations in the diffuse seismic coda*, Science *299*(5606), 547–549.

Chávez-García, F.J., Rodríguez, M., and Stephenson, W.R. (2006), *Subsoil structure using SPAC measurements along a line*, Bull. Seismol. Soc. Am. *96*(2), 729–736.

Chávez-García, F.J., Rodríguez, M., and Stephenson, W.R. (2005), *An alternative approach to the SPAC analysis of microtremors: exploiting stationarity of noise*, Bull. Seismol. Soc. Am. *95*(1), 277–293.

Cho, I., Tada, T., and Shinozaki, Y. (2006), *A generic formulation for microtremor exploration methods using three-component records from a circular array*, Geophys. J. Internat. *165*(1), 236–258.

Ekström, G., Abers, G.A., and Webb, S.C. (2009), *Determination of surface-wave phase velocities across USArray from noise and Aki's spectral formulation*, Geophys. Res. Lett. *36*(18), L18301.

He, X., Xiao, L., Wang, G., Gao, R., Ynag, G., and Yan, S. (2015), *Petrogenesis and Geological Implications of Late Paleozoic Intermediate-Basic Dyke Swarms in Western Junggar*, Earth Sci. *40*(6), 777–796 **(in Chinese)**.

Lin, F., Moschetti, M.P., and Ritzwoller, M.H. (2008), *Surface wave tomography of the western United States from ambient seismic noise: Rayleigh and Love wave phase velocity maps*, Geophys. J. Internat. *173*(1), 281–298.

Lin, F.C., Li, D., Clayton, R.W., and Hollis, D. (2013), *High-resolution 3d shallow crustal structure in Long Beach, California: Application of ambient noise tomography on a dense seismic array*, Geophys. *78*(4), Q45–Q56.

Liu, L., Zhou, J., Yin, F., Feng, M., and Zhang, B. (2014), *The reconnaissance of mineral resources through ASTER data-based image processing, interpreting and ground inspection in the Jiafushaersu Area, West Junggar, China*, J. Earth Sci. *25*(2), 397–406.

Luo, Y., Xia, J., Miller, R.D., Xu, Y., Liu, J., and Liu, Q. (2008), *Rayleigh-wave dispersive energy imaging using a high-resolution linear Radon transform*, Pure Appl. Geophys. *165*(5), 903–922.

Luo, Y., Xu, Y., and Yang, Y. (2012), *Crustal structure beneath the Dabie orogenic belt from ambient noise tomography*, Earth Planet. Sci. Lett. *313*, 12–22.

Margaryan, S., Yokoi, T., and Hayashi, K. (2009), *Experiments on the stability of the spatial autocorrelation method (SPAC) and linear array methods and on the imaginary part of the SPAC coefficients as an indicator of data quality*, Exploration Geophys. *40*(1), 121–131.

Morikawa, H., Sawada, S., and Akamatsu, J. (2004), *A method to estimate phase velocities of Rayleigh waves using microseisms simultaneously observed at two sites*, Bull. Seismol. Soc. Am. *94*(3), 961–976.

Nakata, N., Snieder, R., Tsuji, T., Larner, K., and Matsuoka, T. (2011), *Shear wave imaging from traffic noise using seismic interferometry by cross-coherence*, Geophys. *76*(6), SA97–SA106.

Okada, H. (2003), The microtremor survey method (Vol. 12) (Society of Exploration Geophysicists with the cooperation of Society of Exploration Geophysicists of Japan and Australian Society of Exploration Geophysicists, 2003).

Park, C.B., Miller, R.D., Xia, J., and Ivanov, J. (2007), *Multichannel analysis of surface waves (MASW)—active and passive methods*, The Leading Edge *26*(1), 60–64.

Prieto, G.A., Lawrence, J.F., and Beroza, G.C. (2009), *Anelastic Earth structure from the coherency of the ambient seismic field*, J. Geophys. Res.: Solid Earth (1978–2012) *114*(B7), B07303.

Roux, P., Sabra, K.G., Gerstoft, P., Kuperman, W.A., and Fehler, M.C. (2005), *P-waves from cross-correlation of seismic noise*, Geophys. Res. Lett. *32*(19), L19303.

Sabra, K.G., Gerstoft, P., Roux, P., Kuperman, W.A., and Fehler, M.C. (2005a), *Extracting time-domain Green's function estimates from ambient seismic noise*, Geophys. Res. Lett. *32*(3), L03310.

Sabra, K.G., Gerstoft, P., Roux, P., Kuperman, W.A., and Fehler, M.C. (2005b), *Surface wave tomography from microseisms in Southern California*, Geophys. Res. Lett. *32*(14), L14311.

Schwab, F., and Knopoff, L. (1970), *Surface-wave dispersion computations*, Bull. Seismol. Soc. Am. *60*(2), 321–344.

Shapiro, N.M., and Campillo, M. (2004), *Emergence of broadband Rayleigh waves from correlations of the ambient seismic noise*, Geophys. Res. Lett. *31*(7), L07614.

Shapiro, N.M., Campillo, M., Stehly, L., and Ritzwoller, M.H. (2005), *High-resolution surface-wave tomography from ambient seismic noise*, Science *307*(5715), 1615–1618.

Snieder, R. (2004), *Extracting the Green's function from the correlation of coda waves: A derivation based on stationary phase*, Phys. Rev. E *69*(4), 046610.

Song, Y., Castagna, J.P., Black, R.A., and Knapp, R.W. (1989), Sensitivity of near-surface shear-wave velocity determination from Rayleigh and Love waves: Technical Program with Biographies, SEG, 59th Annual Meeting, Dallas, Texas, 509–512.

Tsai, V.C., and Moschetti, M.P. (2010), *An explicit relationship between time-domain noise correlation and spatial autocorrelation (SPAC) results*, Geophys. J. Internat. *182*(1), 454–460.

Wang, K., Luo, Y., Zhao, K., and Zhang, L. (2014a), *Body waves revealed by spatial stacking on long-term cross-correlation of ambient noise*, J. Earth Sci. *25*(6): 977–984.

Wang, K., Luo, Y., and Li, H.,(2014b), *The nature of ambient noise over a field in western Junggar Basin near Karamay, China*, Proceedings of the 6th International Conference on Environmental and Engineering Geophysics, Xi'an, China, 162–167.

Weaver, R., and Lobkis, O.I. (2001), *Ultrasonics without a source: Thermal fluctuation correlations at MHz frequencies*, Phys. Rev. Lett. *87*(13), 134301.

XIA, J., MILLER, R.D., and PARK, C.B. (1999), *Estimation of near-surface shear-wave velocity by inversion of Rayleigh waves*, Geophys. *64*(3), 691–700.

XIA, J., MILLER, R. D., PARK, C. B. and TIAN, G. (2003), *Inversion of high frequency surface waves with fundamental and higher modes*, J. Appl. Geophys. *52*(1), 45–57.

XIA, J. (2014), *Estimation of near-surface shear-wave velocities and quality factors using multichannel analysis of surface-wave methods*, J. Appl. Geophys. *103*(2), 140–151.

XU, Y., ZHANG, B., LUO, Y., and XIA, J. (2013), *Surface-wave observations after integrating active and passive source data*, The Leading Edge *32*(6), 634–637.

YANG, Y., and RITZWOLLER, M. H. (2008), *Characteristics of ambient seismic noise as a source for surface wave tomography*, Geochemistry Geophysics Geosystems *9*(2), 1256–1256.

YAO, H., VAN DER HILST, R.D., and MAARTEN, V. (2006), *Surface-wave array tomography in SE Tibet from ambient seismic noise and two-station analysis-I. Phase velocity maps*, Geophys. J. Internat. *166*(2), 732–744.

YAO, H. and VAN DER HILST, R.D. (2009), *Analysis of ambient noise energy distribution and phase velocity bias in ambient noise tomography*, *with application to SE Tibet*, Geophys. J. Internat. *179*(2), 1113–1132.

(Received March 5, 2015, revised July 28, 2015, accepted July 29, 2015, Published online August 12, 2015)